Postprint of: Nosko O., Borrajo-Pelaez R., Hedström P., Olofsson U., Porosity and shape of airborne wear microparticles generated by sliding contact between a low-metallic friction material and a cast iron, Journal of Aerosol Science, Vol. 113 (2017), pp. 130-140, DOI: 10.1016/j.jaerosci.2017.07.015

Porosity and shape of airborne wear microparticles generated by sliding contact between a low-metallic friction material and a cast iron

Oleksii Nosko[a*], Rafael Borrajo-Pelaez[b], Peter Hedström[b], Ulf Olofsson[a]

[a] Department of Machine Design; [b] Department of Materials Science and Engineering, KTH Royal Institute of Technology, Stockholm, 100 44, Sweden

The wear of brakes in transport vehicles is one of the main anthropogenic sources of airborne particulate matter in urban environments. The present study deals with the characterisation of airborne wear microparticles from a low-metallic friction material / cast iron pair used in car brakes. Particles were generated by a pin-on-disc machine in a sealed chamber at sliding velocity of 1.3 m/s and contact pressure of 1.5 MPa. They were collected on filters in an electrical low pressure impactor, and an investigation was conducted to quantify their shape and porosity. Scanning electron microscopy revealed that most of the 0.1−0.9 µm particles are flakes and have a breadth-to-length aspect ratio of 0.7 ± 0.2. Particle porosity was determined by milling particles with a focused ion beam and subsequent analysis of the exposed particle cross-sections. Most of the 0.3−6.2 µm particles were revealed to have porosity of 9 ± 6 %. Analysis of the relationship between effective particle density, particle material density, dynamic shape factor and porosity showed that the shape factor has a stronger influence on the effective density of airborne wear particles than the porosity factor. The obtained results are useful for accurate prediction of particle behaviour in the atmosphere and in the human respiratory system.

Keywords: pin-on-disc; airborne wear particles; aerosol measurement; particle porosity; particle shape; dynamic shape factor.

Given name	Family name
Oleksii	Nosko
Rafael	Borrajo-Pelaez
Peter	Hedström
Ulf	Olofsson

[*] Corresponding author. E-mail: nosko@kth.se (O. Nosko).

1. Introduction

Airborne particulate matter penetrates the human body through breathing, drinking, eating, and skin contact. The penetration of microscopic and submicron particles may have adverse health effects in the form of asthma, lung cancer, cardiovascular disease, respiratory diseases, and skin diseases (Pope et al., 2002; Oberdörster et al., 2005). People living in urban environments are subject to higher health risks due to various anthropogenic sources of airborne particles such as the burning of fossil fuels to generate electricity, construction, demolition, and road transportation (Kumar et al., 2013; Vu et al., 2015). The impact of the latter is specifically significant in the vicinity of traffic arteries (Furusjö et al., 2007; Pant and Harrison, 2013). Studies by Thorpe and Harrison (2008), Gietl et al. (2010) and Amato et al. (2014) showed that one of the main traffic-related sources of airborne particles is the wear of brakes in transport vehicles. Modern cars are equipped with disc brakes which provide braking through the friction of two pads against a disc. The disc material is usually cast iron, whereas most of the pad materials fall into three classes: low-metallic (LM), non-asbestos organic (NAO), and semi-metallic (SM). During braking, wear particles are emitted from the friction surfaces of the pads and disc. Some of these particles become airborne and are released to the environment.

Grigoratos and Martini (2015) reviewed many studies on airborne wear particle emissions from car brake materials. Garg et al. (2000) investigated the generation of particulate matter by brakes with NAO and SM pads, focusing on particle emission rate, size distribution, and elemental composition. Particle size distributions of wear debris from brakes with LM, NAO and SM pads were measured by Sanders et al. (2003). Schauer et al. (2006) presented a report on the characterisation of metals emitted from motor vehicles, including brake wear emissions. Iijima et al. (2007) investigated abrasion dusts from brakes with NAO pads, considering size distribution and elemental composition. Wahlström et al. (2010a, 2010b) conducted studies of particulate matter emissions from LM and NAO materials against cast iron. The particles were analysed for concentration, size distribution, shape, and elemental composition. Kukutschová et al. (2011) performed a study of particle emissions from brakes with LM pads. The particle concentration, size distribution, chemistry, mutagenicity, and toxicity were analysed. Hagino et al. (2015, 2016) investigated mass concentrations of wear particles from brake dynamometer imitating real driving conditions. Alemani et al. (2016) and Nosko and Olofsson (2017a,b) performed pin-on-disc studies of wear particles generated by the friction of LM and NAO materials against cast iron. Particle emission rate, size distribution and density were investigated, taking into account the influence of temperature.

The above literature review suggests that airborne wear particles generated by car brakes have been thoroughly investigated in terms of emission rate, size distribution, density, and

chemistry. Nonetheless, quantitative information about their porosity and shape is still lacking. Particle porosity serves as a link between particle density and the density of the particle material (DeCarlo et al., 2004). It is also related to particle chemical reactivity. On the other hand, particle shape has a significant influence on the drag force acting on the particle, which is described by the dynamic shape factor (Fuchs, 1964). Both particle porosity and shape affect the so-called effective particle density (Kelly and McMurry, 1992), another important characteristic necessary to predict the dynamic behaviour of particles in the atmosphere and in the human respiratory system.

The aim of this study was to quantitatively characterise the porosity and shape of airborne wear particles emitted from a LM / cast iron pair used in car brakes.

2. Basic definitions and relationships

The geometry of a particle is characterised by the breadth B, which is the minimum distance between two parallel tangents to the particle profile, and the length L, which is similar to the breadth but taken in the perpendicular direction (Davies, 1979). The equivalent 2D particle diameter can then be expressed as

$$d = \sqrt{BL}$$

Furthermore, the aspect ratio is

$$r = \frac{B}{L}$$

The particle material density ρ_m is defined as the ratio of the particle mass m to the volume V_s of the solid material in the particle:

$$\rho_\mathrm{m} = \frac{m}{V_\mathrm{s}}$$

The particle density ρ_p takes the internal voids of the particle into account:

$$\rho_\mathrm{p} = \frac{m}{V_\mathrm{s} + V_\mathrm{v}}$$

where V_v is the volume of the internal voids. The particle porosity ϕ is defined as

$$\phi = \frac{V_\mathrm{v}}{V_\mathrm{s} + V_\mathrm{v}} \tag{1}$$

and ρ_m and ρ_p are linked by the following equation (DeCarlo et al., 2004):

$$\rho_\mathrm{p} = (1 - \phi)\rho_\mathrm{m} \tag{2}$$

The effective particle density ρ_e is used to describe the aerosol dynamic behaviour. It is often defined based on the following relationship between the particle mobility diameter d_b and aerodynamic diameter d_a (Schmid et al., 2007):

$$\rho_e d_b^2 \, C_c(d_b) = \rho_0 d_a^2 \, C_c(d_a)$$

where ρ_0 = 1 g/cm^3 and $C_c(\cdot)$ is the slip correction factor.

The dynamic shape factor κ is defined as the ratio of the drag force on the non-spherical particle to the drag force on its volume equivalent sphere, assuming that both move at the same velocity with respect to the atmosphere (Fuchs, 1964). Fig.1 shows approximate values of κ for some idealised particles (Johnson et al., 1987; Kasper, 1982, 1985; Niida and Ohtsuka, 1996). The variation in κ is due to the different possible orientations of the particles with respect to the air flow direction. The value of κ is about 1 to 1.2 for the idealised rounded / angular particles. For the idealised agglomerates κ varies from 1 to 1.5. By contrast, the idealised flaky particles, with a thickness-to-diameter ratio of 0.1, have a considerably larger κ in the range of 1.3 to 2.2.

According to experimental data obtained by Zelenyuk et al. (2006) for 0.1–1 μm aerosol particles of polystyrene latex, ammonium sulphate and sodium chloride with various irregular shapes, as well as theoretical analysis by DeCarlo et al. (2004), the relationship between ρ_e and ρ_p can be represented in the form

$$\frac{\rho_e}{\rho_p} \approx \frac{1}{\kappa^2} \tag{3}$$

From Eqs.(2) and (3) it follows that

$$\frac{\rho_m}{\rho_e} \approx \frac{\kappa^2}{1-\phi} \tag{4}$$

The derived Eq.(4) describes the combined effect of the particle porosity ϕ and shape (κ) on the effective particle density ρ_e.

3. Research methodology

3.1. Generation and collection of particles

Airborne wear particles were generated by the pin-on-disc machine depicted in Fig.2. This set-up was proposed by Olofsson et al. (2009, 2011, 2013). The pin sample was a cylinder with a diameter of 10 mm. A dead weight pressed it against a horizontally positioned disc, providing a contact pressure of 1.5 MPa. The average friction radius was 25 mm. The disc was driven by a motor with a constant velocity of 1.3 m/s at the average friction radius. Temperature was measured in the disc using a chromel–alumel thermocouple.

The pin sample and disc were milled from passenger car brake LM pad and cast iron disc. The LM is representative for the European market, with a phenolic resin binder and different reinforcements and abrasives. The cast iron is a perlitic lamellar cast iron. The elemental

compositions of the LM, reported by Alemani et al. (2016), and the cast iron, reported by Matějka et al. (2016), are presented in Table 1.

Table 1. Elemental compositions of the friction materials, wt. %

	Mg	Al	Si	Mn	P	S	K	Ca	Ti	Cr	Fe	Cu	Zn	Sr	Zr	Sn	Bi	C	F
LM	10.4	9.1	5.8		0.9	5.2	0.67	5	0.17	3.3	7.1	5.4	12.5	0.01	0.14	8.8	0.81	22.4	2.1
Cast iron			1.7	0.57	0.03	0.26				0.2	93.6	0.24						3.4	

The pin-on-disc machine was located in a sealed chamber to avoid external sources of particles. Room air was drawn in by a fan and entered the chamber through a HEPA filter and an inlet opening. The air flow was 2.2 L/s. The air flow inside the chamber picked up particles generated by the friction of the pin sample on the disc and carried them to the air outlet. The particles coming out of the chamber were collected on aluminium filters placed inside a Dekati Electrical Low Pressure Impactor 2E10-10 (ELPI+).

The test duration was 3 hours. During the first 30 min, transient processes were observed, including rise of the disc temperature and changes in the ELPI+ particle size distribution. After the stationary friction was reached, the disc temperature fluctuated about 270 °C, while the ELPI+ indicated the presence of particles in the entire measurement range from 0.006 to 10 μm. The normalised particle concentration was of the order 10^6, 10^3, 10 and 1 no/($cm^3 \Delta \log D_p$) for particle diameter of 0.01, 0.1, 1 and 10 μm, respectively. A detailed description of the influence of temperature and friction duration on the particle size distribution for the LM / cast iron pair can be found in Nosko and Olofsson (2017a,b).

3.2. Particle sectioning

Some of the particles accumulated on the filters underwent sectioning in a dual-beam microscope FEI Nova Nanolab 600, equipped with a gallium focused ion beam and a field emission gun scanning electron microscope (SEM).

The sample preparation procedure consisted of the deposition of a gold coating and a platinum patch over the substrate containing the particles. The gold coating, with a thickness of several nanometres, was produced in a plasma coater JEOL JFC-1300 in order to ensure the conductivity of the specimen and to encapsulate it. The platinum patch was produced by means of beam chemistry deposition inside the microscope over the areas of the sample that needed to be

sectioned. Its purpose was to protect the region of study from undesired etching resulting from exposure to the ion beam during beam tuning.

The platinum patch was deposited over the specimen in two stages. First, the sample was placed in the direction normal to the SEM beam and a platinum layer of 0.1 μm was deposited over the region of study. The deposition of this layer occurred upon injection of a precursor gas close to the region of study using a gas injection system. The region of study was then irradiated with the electron beam (e-beam). The energy of the electrons in the beam broke the precursor gas molecules and produced platinum deposition. Fig.3a shows a SEM image of a particle cluster covered with the e-beam platinum layer. At the second stage, the sample was positioned in the direction normal to the ion beam (i-beam) as shown in Fig.4. An extra platinum layer of 1–2 μm was deposited from the same precursor gas, this time upon i-beam irradiation. Fig.3b shows a SEM image of the particle cluster after the i-beam platinum deposition. Notice that the sample stage is tilted 52° to be placed normal to the i-beam direction.

The sample was milled step-by-step using the i-beam. At each step, a prismatic volume of the sample was removed, exposing the subsequent cross-section of the particle cluster. The cross-section was then imaged with the SEM, as illustrated in Fig.3c. The thickness of the removed volume, i.e. the distance between two consecutive cross-sections, was set in accordance with the particle cluster size and was constant within the sectioning procedure.

3.3. Processing of the particle cross-section images

Each particle cross-section image was processed in the following way. The initial image (Fig.5a) was cleaned to remove the background and thus frame the particle (Fig.5b). Image thresholding was then performed to contour the voids in the particle (Fig.5c). At the final stage, the solid material of the particle was coloured grey (Fig.5d). This transformed the initial image into three domains: ‘background’, coloured in white; ‘solid material’, coloured in grey; ‘voids’, coloured in black.

The porosity ϕ of a particle was determined by analysing a number n of its cross-section images. Each i-th image was processed following the procedure described above. The domains of ‘voids’ and ‘solid material’ were obtained, and their areas A_{vi} and A_{si} were determined. Finally, ϕ was calculated by the formula

$$\phi = \sum_{i=1}^{n} A_{\mathrm{v}i} \Big/ \sum_{i=1}^{n} \left(A_{\mathrm{s}i} + A_{\mathrm{v}i}\right)$$

which is an approximation of Eq.(1).

4. Results

SEM analysis showed that the particles have various shapes, as illustrated in Fig.6. The primary particles can be rounded / angular (Fig.6a), flaky (Fig.6b), or acicular (Fig.6c). There are also agglomerated particles (Fig.6d).

Fig.7 presents a micrograph of particles collected on a filter. The micrograph contains several hundred particles, and the resolution and contrast are high enough to distinguish boundaries of overlying particles. A statistical analysis of the shape and aspect ratio r was performed for 200 randomly selected particles with d from 0.1 to 0.9 μm. It was found that about 60 % of the particles are flakes. There are also a noticeable number of rounded / angular and agglomerated particles, while acicular particles are rare. Fig.8 shows the distribution of the relative frequency of r. The average value of r is 0.7, and 83 % of the particles have r in the range 0.7 ± 0.2.

The porosity ϕ of 20 randomly selected particles with d ranging from 0.3 to 6.2 μm was determined. Of them, 16 particles were primary and 4 particles were agglomerates. In the calculations, the number n of the cross-section images varied between 2 and 5. Fig.9 presents the relationship between ϕ and d obtained for each particle. The value of ϕ is in the range of 9 ± 6 % for a total of 12 out of the 20 particles considered. Examples of a completely dense particle (ϕ = 0), a porous primary particle with ϕ = 9 %, and an agglomerated particle with ϕ = 22 % are indicated in Fig.9 by ‘A’, ‘B’, and ‘C’, respectively. In addition, cross-section images of the particles ‘A’ and ‘B’ are shown in Fig.10. The particle ‘C’ was presented in Fig.5.

5. Discussion

The shape of airborne wear particles was previously investigated by Wahlström et al. (2010b) who conducted a pin-on-disc study of LM and NAO materials. SEM analysis of the collected microparticles showed that most of them had a flaky shape. Kukutschová et al. (2011) also investigated particulate matter generated by a brake dynamometer with LM pads. Particles varying between 0.037 and 9.5 μm in aerodynamic diameter were collected on filters and analysed using SEM and transmission electron microscopy. The analysis revealed the presence of nanoscale particles in the form of agglomerates, while a noticeable number of microparticles were flakes. The results from the present study are similar to the described results, showing predominantly flaky microparticles with a fraction of about 60 %. In addition, it was found that the particles have an elongated shape with the aspect ratio r of 0.7 ± 0.2 (see Fig.8).

To the best of our knowledge, there are no previously published data on the porosity of airborne wear particles. The current study shows that the porosity ϕ of these particles is 9 ± 6 %. According to Fig.9, there is a large scatter in ϕ, from completely dense particles (see Fig.10, particle ‘A’) to particles with ϕ above 20 % (see Fig.5). Agglomerated particles have voids between

their sub-particles, and it is natural to expect them to have a certain level of porosity. The primary particles under study, however, were also revealed to be porous (see Fig.10, particle 'B').

Alemani et al. (2016) investigated airborne wear particles generated by friction pairs similar to that considered in the present study. The particulate matter was collected on ELPI+ filters and analysed for elemental composition by energy-dispersive X-ray spectroscopy. Based on the elemental composition, the material density ρ_m of 0.06–10 μm aerodynamic diameter particles was calculated to be about 2.6 g/cm^3. Nosko and Olofsson (2017b) studied the effective density ρ_e of airborne wear particles from the same friction pairs. It was found that ρ_e of 0.006–10 μm particles is about 0.75 g/cm^3, i.e. the ratio $\rho_m/\rho_e \approx 3.5$. Such a large difference between ρ_e and ρ_m was hypothesised to be caused by the particle porosity and shape. If we substitute $\rho_m/\rho_e = 3.5$ and $\phi = 0.09$ in Eq.(4), we obtain the dynamic shape factor $\kappa = 1.78$. This value lies close to the midpoint of the range $\kappa = 1.4$–2 for the idealised flaky particle with $r = 1/2$ (see Fig.1), and it also agrees well with $\kappa = 1.88$ obtained by Cheng et al. (1988) for flaky aerosol microparticles of talc with a thickness-to-diameter ratio of about 0.1. Thus, the large difference between ρ_e and ρ_m can be explained by the predominantly flaky shape of the particles. The porosity factor is of comparably minor importance.

6. Conclusions

This study provides a quantitative characterisation of the porosity and shape of airborne wear microparticles generated by a low-metallic friction material / cast iron pair used in car brakes. The main findings can be summarised as follows:

1. The particles have various shapes: rounded / angular, flaky, acicular, and agglomerated. Flaky particles are predominant, with a fraction of about 60 %.
2. Most particles within the diameter range of 0.1−0.9 μm have an elongated shape with a breadth-to-length aspect ratio of 0.7 ± 0.2.
3. The porosity of most of the 0.3−6.2 μm particles is 9 ± 6 %. There are also completely dense particles as well as particles with porosity above 20 %.
4. The shape factor has a stronger influence on the effective particle density than the porosity factor.

Vitae

Oleksii Nosko received the Doctor's degree in Tribology at Bauman Moscow State Technical University in 2010 and the Ph.D. in Mechanical Engineering at Saitama University in 2013. His

main research interests include measurement and simulation of temperatures at sliding contacts, thermo-mechanical friction problems, and airborne particle emissions from sliding contacts.

Rafael Borrajo-Pelaez completed a Ph.D. in Aerospace Engineering at University of California Irvine, specializing in Space Propulsion and Material Science. His research focuses on aerosols, in particular the electrospray atomization of liquids applied to colloid thrusters and the transformation of material properties via energetic bombardment with electrospray nanoparticles. He worked at Yale University on the development of methods for the analysis of proteins and detection of explosives through aerosol characterization with ion mobility and mass spectrometry. He worked as a post-doctoral researcher on Metallurgy and Advanced Materials Characterization at KTH and he is currently a Space Propulsion engineer at OHB Sweden.

Peter Hedström obtained his PhD in Engineering Materials from Luleå University of Technology in 2007. He subsequently worked at the metallurgical research institute – Swerea MEFOS, before taking up a position at KTH Royal Institute of Technology in 2008. He is currently employed as Assistant Professor at the Department of Materials Science and Engineering, KTH.

Ulf Olofsson is a Professor in Tribology at KTH Royal Institute of Technology since 2006. He received the Ph.D. in 1996 on a thesis on wear as failure mechanism in boundary lubricated rolling bearings. His main research interests include interfaces and especially simulation and prediction of friction and wear, mainly applied to problems in mechanical, automotive and railway engineering. New research interests include friction modifiers in rolling sliding contacts and joints, airborne particles from wear processes in disc brakes, tyre to road interaction, and human touch tribology.

Acknowledgement

This work was supported by the European Union Seventh Framework Programme (FP-PEOPLE-2012-IAPP) under the Rebrake Project [grant number 324385].

The assistance of Brembo S.p.A. and Mr Guido Perricone is gratefully acknowledged.

References

1. Alemani, M., Nosko, O., Metinoz, I., & Olofsson, U. (2016). A study on emission of airborne wear particles from car brake friction pairs. *SAE International Journal of Materials and Manufacturing*, 9 (1), 147–157.

2. Amato, F., Cassee, F.R., Denier van der Gon, H.A.C., Gehrig, R., Gustafsson, M., Hafner, W., … Querol, X. (2014). Urban air quality: The challenge of traffic non-exhaust emissions. *Journal of Hazardous Materials*, 275, 31–36.
3. Cheng, Y.-S., Yeh, H.-C., & Allen, M.D. (1988). Dynamic shape factor of a plate-like particle. *Aerosol Science and Technology*, 8 (2), 109−123.
4. Davies, C.N. (1979). Particle–fluid interaction. *Journal of Aerosol Science*, 10 (5), 477–513.
5. DeCarlo, P.F., Slowik, J.G., Worsnop, D.R., Davidovits, P., & Jimenez, J.L. (2004). Particle morphology and density characterization by combined mobility and aerodynamic diameter measurements. Part 1: Theory. *Aerosol Science and Technology*, 38 (12), 1185–1205.
6. Fuchs, N.A. (1964). *The mechanics of aerosols*. New York: Pergamon.
7. Furusjö, E., Sternbeck, J., & Cousins, A.P. (2007). PM10 source characterization at urban and highway roadside locations. *Science of the Total Environment*, 387 (1–3), 206–219.
8. Garg, B.D., Cadle, S.H., Mulawa, P.A., & Groblicki, P.J. (2000). Brake wear particulate matter emissions. *Environmental Science and Technology*, 34 (21), 4463–4469.
9. Gietl, J.K., Lawrence, R., Thorpe, A.J., & Harrison, R.M. (2010). Identification of brake wear particles and derivation of a quantitative tracer for brake dust at a major road. *Atmospheric Environment*, 44 (2), 141–146.
10. Grigoratos, T., & Martini, G. (2015). Brake wear particle emissions: A review. *Environmental Science and Pollution Research*, 22 (4), 2491–2504.
11. Hagino, H., Oyama, M., & Sasaki, S. (2015). Airborne brake wear particle emission due to braking and accelerating. *Wear*, 334–335, 44–48.
12. Hagino, H., Oyama, M., & Sasaki, S. (2016). Laboratory testing of airborne wear particle emissions using a dynomometer system under urban city driving cycles. *Atmospheric Environment*, 131, 269–278.
13. Iijima, A., Sato, K., Yano, K., Tago, H., Kato, M., Kimura, H., & Furuta, N. (2007). Particle size and composition distribution analysis of automotive brake abrasion dusts for the evaluation of antimony sources of airborne particulate matter. *Atmospheric Environment*, 41 (23), 4908–4919.
14. Johnson, D.L., Leith, D., & Reist, P.C. (1987). Drag on non-spherical, orthotropic aerosol particles. *Journal of Aerosol Science*, 18 (1), 87–97.
15. Kasper, G. (1982). Dynamics and measurement of smokes. I Size characterization of nonspherical particles. *Aerosol Science and Technology*, 1 (2), 187–199.
16. Kasper, G. (1985). Measurements of viscous drag on cylinders and chains of spheres with aspect ratios between 2 and 50. *Journal of Aerosol Science*, 16 (6), 535–556.

17. Kelly, W.P., & McMurry, P.H. (1992). Measurement of particle density by inertial classification of differential mobility analyzer-generated monodisperse aerosols. *Aerosol Science and Technology*, 17 (3), 199–212.
18. Kukutschová, J., Moravec, P., Tomášek, V., Matějka, V., Smolík, J., Schwarz, J., … Filip, P. (2011). On airborne nano/micro-sized wear particles released from low-metallic automotive brakes. *Environmental Pollution*, 159 (4), 998–1006.
19. Kumar, P., Pirjola, L., Ketzel, M., & Harrison, R.M. (2013). Nanoparticle emissions from 11 non-vehicle exhaust sources — A review. *Atmospheric Environment*, 67, 252–277.
20. Matějka, V., Metinöz, I., Alemani, M., Wahlström, J., Bonfanti, A., Oloffson, U., & Perricone, G. (2016). Dependency of PM10 particles emission on stability of friction coefficient and character of friction surface. Proceedings of Europe's Braking Conference and Exhibition, EB2016-MDS-009.
21. Niida, T., & Ohtsuka, S. (1997). Dynamic shape factors of regular shaped agglomerates and estimation based on agglomerate symmetry: For rectangular parallelepiped, V- and W-shaped, hexagonal and H-shaped agglomerates. *KONA*, 15, 202–211.
22. Nosko, O., & Olofsson, U. (2017a). Quantification of ultrafine airborne particulate matter generated by the wear of car brake materials. *Wear*, 374−375, 92−96.
23. Nosko, O., & Olofsson, U. (2017b). Effective density of airborne wear particles from car brake materials. *Journal of Aerosol Science*, 107, 94−106.
24. Oberdörster, G., Maynard, A., Donaldson, K., Castranova, V., Fitzpatrick, J., Ausman, K., … Yang H. (2005). Principles for characterizing the potential human health effects from exposure to nanomaterials: Elements of a screening strategy. *Particle and Fibre Toxicology*, 2, 8.
25. Olofsson, U., Olander, L., & Jansson, A. (2009). A study of airborne wear particles generated from a sliding contact. *Journal of Tribology*, 131 (4), 044503.
26. Olofsson, U. (2011). A study of airborne wear particles generated from the train traffic — Block braking simulation in a pin-on-disc machine. *Wear*, 271 (1–2), 86–91.
27. Olofsson, U., & Olander, L. (2013). On the identification of wear modes and transitions using airborne wear particles. *Tribology International*, 59, 104–113.
28. Pant, P., & Harrison, R.M. (2013). Estimation of the contribution of road traffic emissions to particulate matter concentrations from field measurements: A review. *Atmospheric Environment*, 77, 78–97.
29. Pope, C.A., Burnett, R.T., Thun, M.J., Calle, E.E., Krewski, D., Ito, K., & Thurston, G.D. (2002). Lung cancer, cardiopulmonary mortality, and long-term exposure to fine particulate air pollution. *The Journal of the American Medical Association*, 287 (9), 1132–1141.

30. Sanders, P.G., Xu, N., Dalka, T.M., & Maricq, M.M. (2003). Airborne brake wear debris: Size distributions, composition, and a comparison of dynamometer and vehicle tests. *Environmental Science and Technology*, 37 (18), 4060–4069.
31. Schauer, J.J., Lough, G.C., Shafer, M.M., Christensen, W.F., Arndt, M.F., DeMinter, J.T., & Park, J.-S. (2006). Characterization of emissions of metals emitted from motor vehicles. Health Effects Institute Research Report, 133.
32. Schmid, O., Karg, E., Hagen, D.E., Whitefield, P.D., & Ferron, G.A. (2007). On the effective density of non-spherical particles as derived from combined measurements of aerodynamic and mobility equivalent size. *Journal of Aerosol Science*, 38 (4), 431–443.
33. Thorpe, A., & Harrison, R.M. (2008). Sources and properties of non-exhaust particulate matter from road traffic: A review. *Science of the Total Environment*, 400 (1–3), 270–282.
34. Vu, T.V., Delgado-Saborit, J.M., & Harrison, R.M. (2015). Review: Particle number size distributions from seven major sources and implications for source apportionment studies. *Atmospheric Environment*, 122, 114–132.
35. Wahlström, J., Söderberg, A., Olander, L., Olofsson, U., & Jansson, A. (2010a). Airborne wear particles from passenger car disc brakes: A comparison of measurements from field tests, a disc brake assembly test stand, and a pin-on-disc machine. *Proceedings of the Institution of Mechanical Engineers. Part J: Journal of Engineering Tribology*, 224, 179–188.
36. Wahlström, J., Olander, L., & Olofsson U. (2010b). Size, shape, and elemental composition of airborne wear particles from disc brake materials. *Tribology Letters*, 38 (1), 15–24.
37. Zelenyuk, A., Cai, Y., & Imre, D. (2006). From agglomerates of spheres to irregularly shaped particles: Determination of dynamic shape factors from measurements of mobility and vacuum aerodynamic diameters. *Aerosol Science and Technology*, 40 (3), 197–217.

Figure captions

All figures — colour online only.

Fig.1. Dynamic shape factor κ and aspect ratio r of idealised particles

Fig.2. Schematic of the experimental set-up for particle generation and collection

Fig.3. SEM images of a particle cluster: (a) after the deposition of an e-beam platinum patch; (b) after the deposition of an i-beam platinum patch; (c) during i-beam etching

Fig.4. Schematic of the relative position between the sample, the e-beam and the i-beam

Fig.5. Processing of the particle cross-section image: (a) initial image; (b) removal of the background; (c) black colouring of the voids; (d) grey colouring of the solid material

Fig.6. Particle shapes: (a) rounded / angular; (b) flaky; (c) acicular; (d) agglomerated

Fig.7. SEM micrograph of particles collected on a filter

Fig.8. Distribution of the relative frequency of the particle aspect ratio r

Fig.9. Particle porosity ϕ vs. diameter d: • primary particle; ▲ agglomerated particle; (A) example of a completely dense particle; (B) example of a porous primary particle; (C) example of an agglomerated particle

Fig.10. Typical cross-section images of the primary particles: (A) completely dense particle; (B) porous particle

Fig. 1

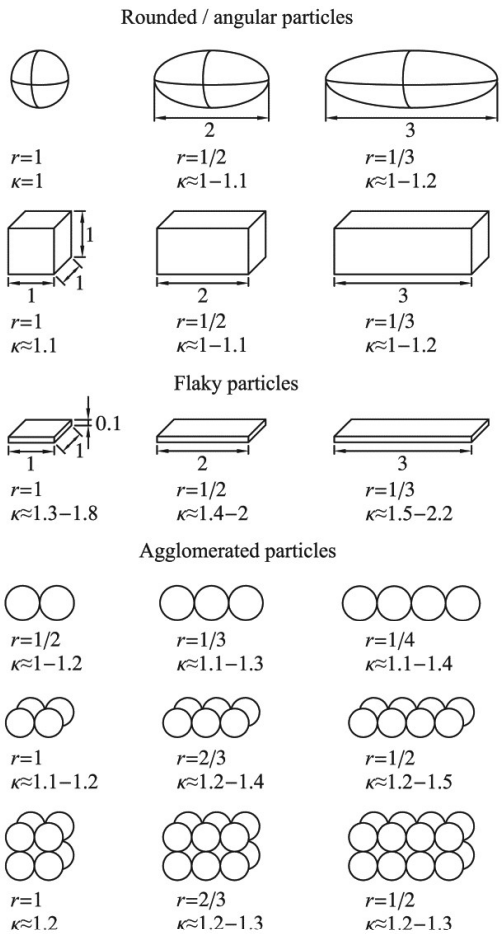

Fig.2

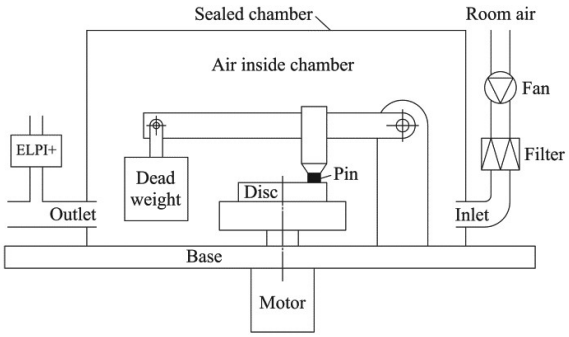

Fig.3

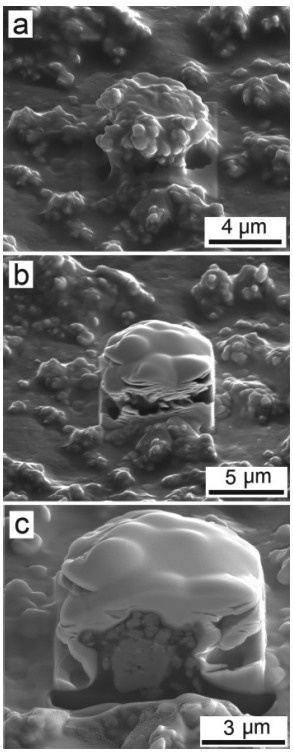

Fig.4

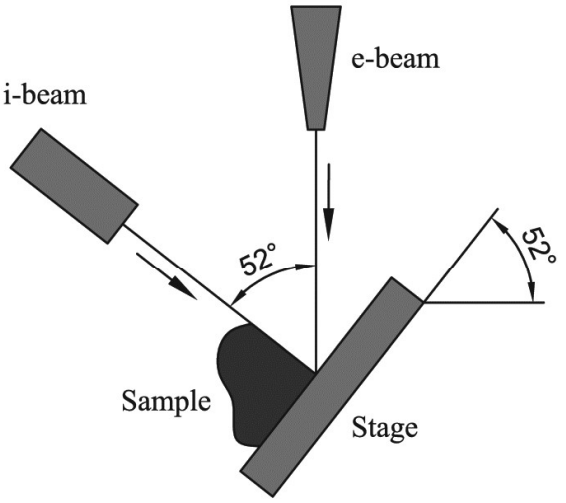

Fig.5

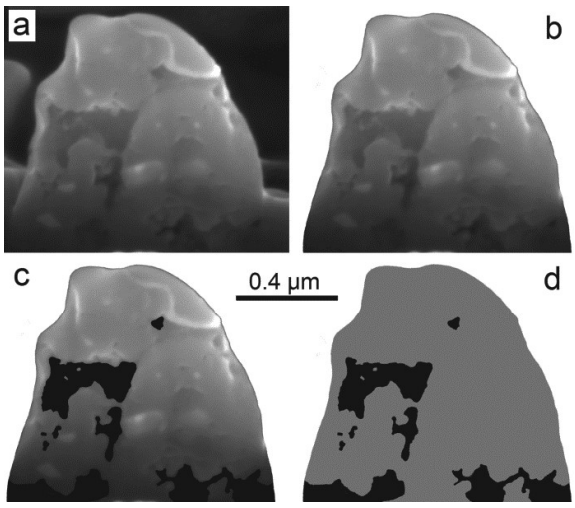

Fig.6

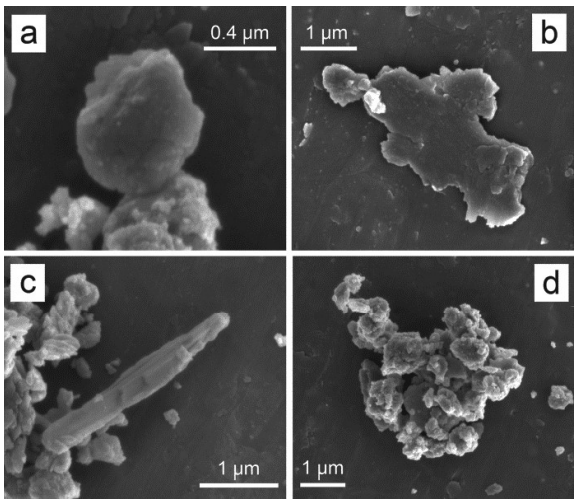

Fig.7

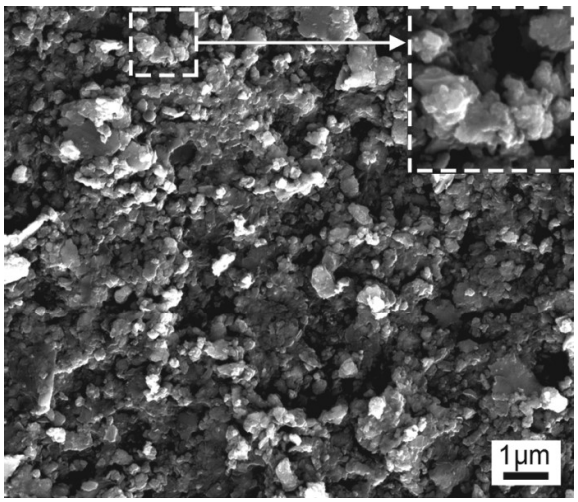

Fig.8

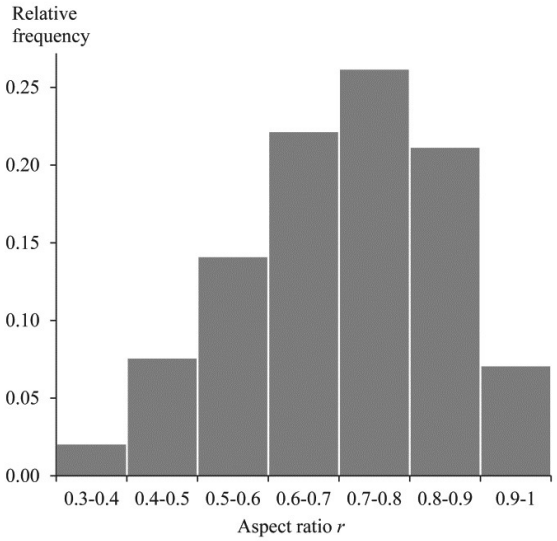

Fig.9

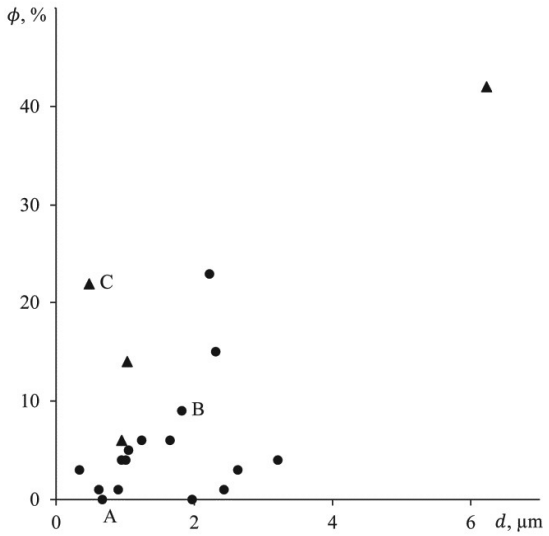

Fig.10

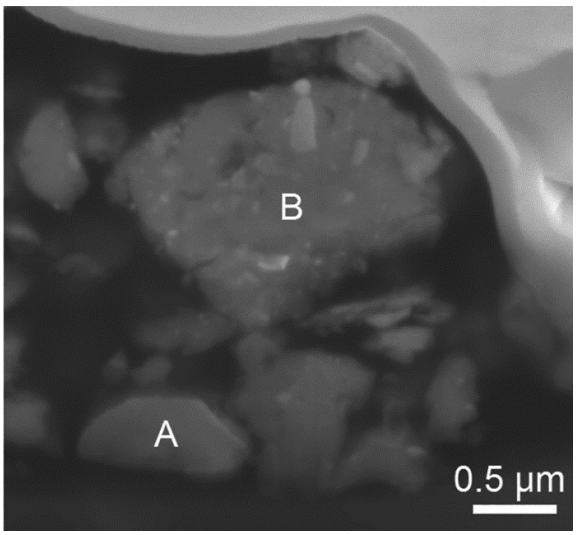

Rounded / angular particles

$r=1$
$\kappa=1$

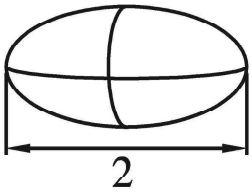

$r=1/2$
$\kappa\approx1-1.1$

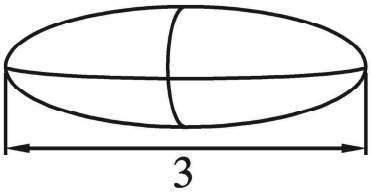

$r=1/3$
$\kappa\approx1-1.2$

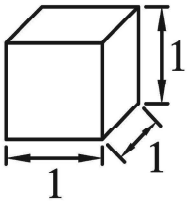

$r=1$
$\kappa\approx1.1$

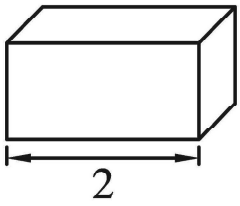

$r=1/2$
$\kappa\approx1-1.1$

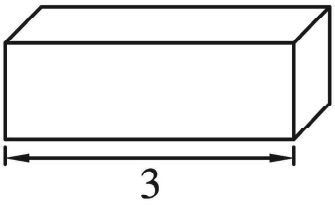

$r=1/3$
$\kappa\approx1-1.2$

Flaky particlcs

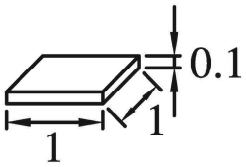

$r=1$
$\kappa\approx1.3-1.8$

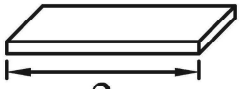

$r=1/2$
$\kappa\approx1.4-2$

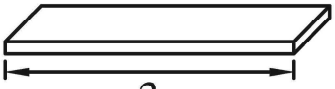

$r=1/3$
$\kappa\approx1.5-2.2$

Agglomerated particles

$r=1/2$
$\kappa\approx1-1.2$

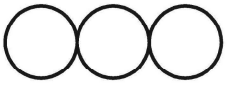

$r=1/3$
$\kappa\approx1.1-1.3$

$r=1/4$
$\kappa\approx1.1-1.4$

$r=1$
$\kappa\approx1.1-1.2$

$r=2/3$
$\kappa\approx1.2-1.4$

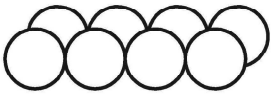

$r=1/2$
$\kappa\approx1.2-1.5$

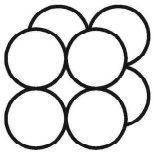

$r=1$
$\kappa\approx1.2$

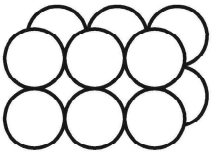

$r=2/3$
$\kappa\approx1.2-1.3$

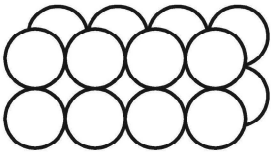

$r=1/2$
$\kappa\approx1.2-1.3$

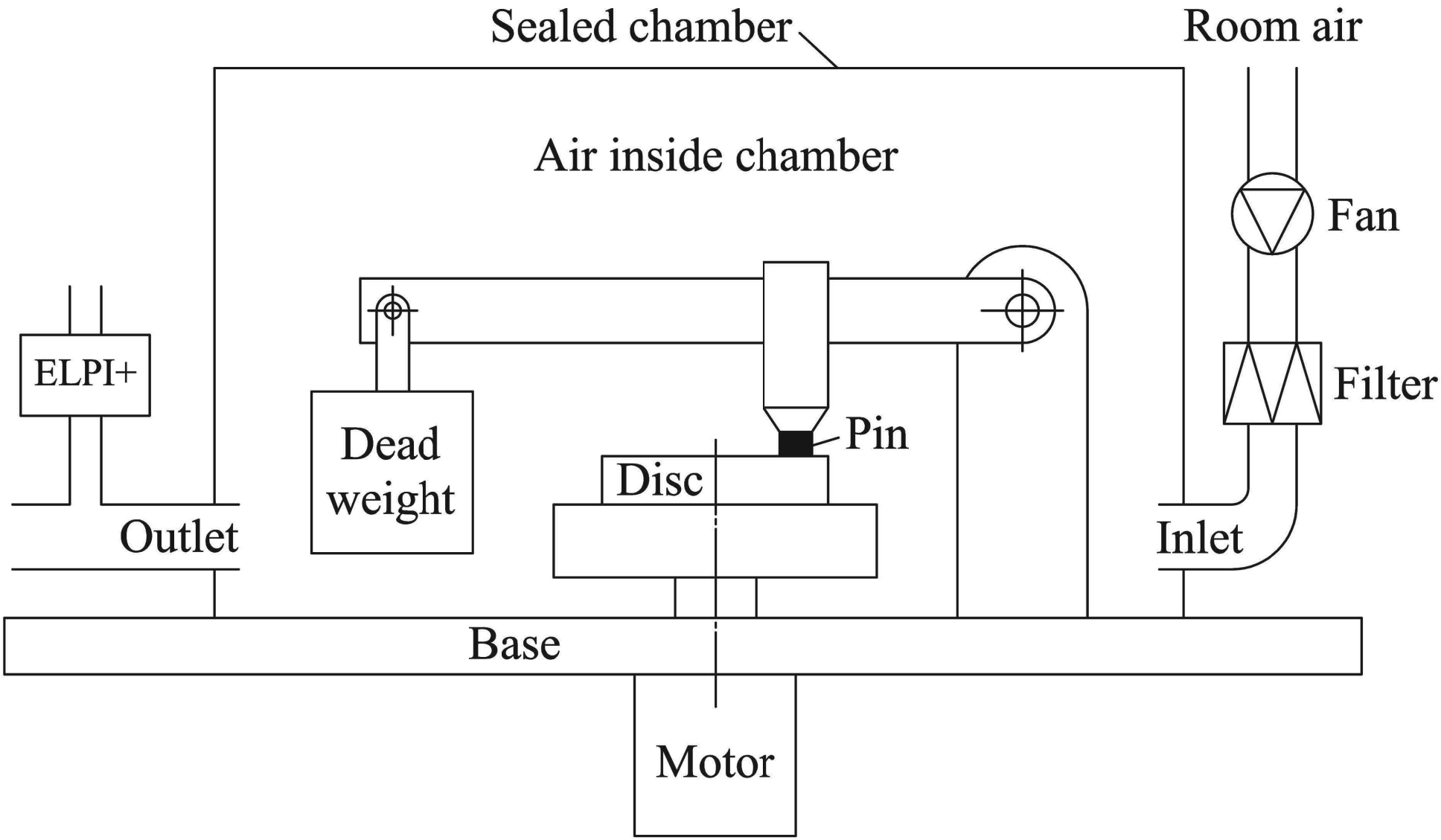
Sealed chamber
Room air
Air inside chamber
Fan
ELPI+
Filter
Dead
weight
Pin
Disc
Outlet
Inlet
Base
Motor

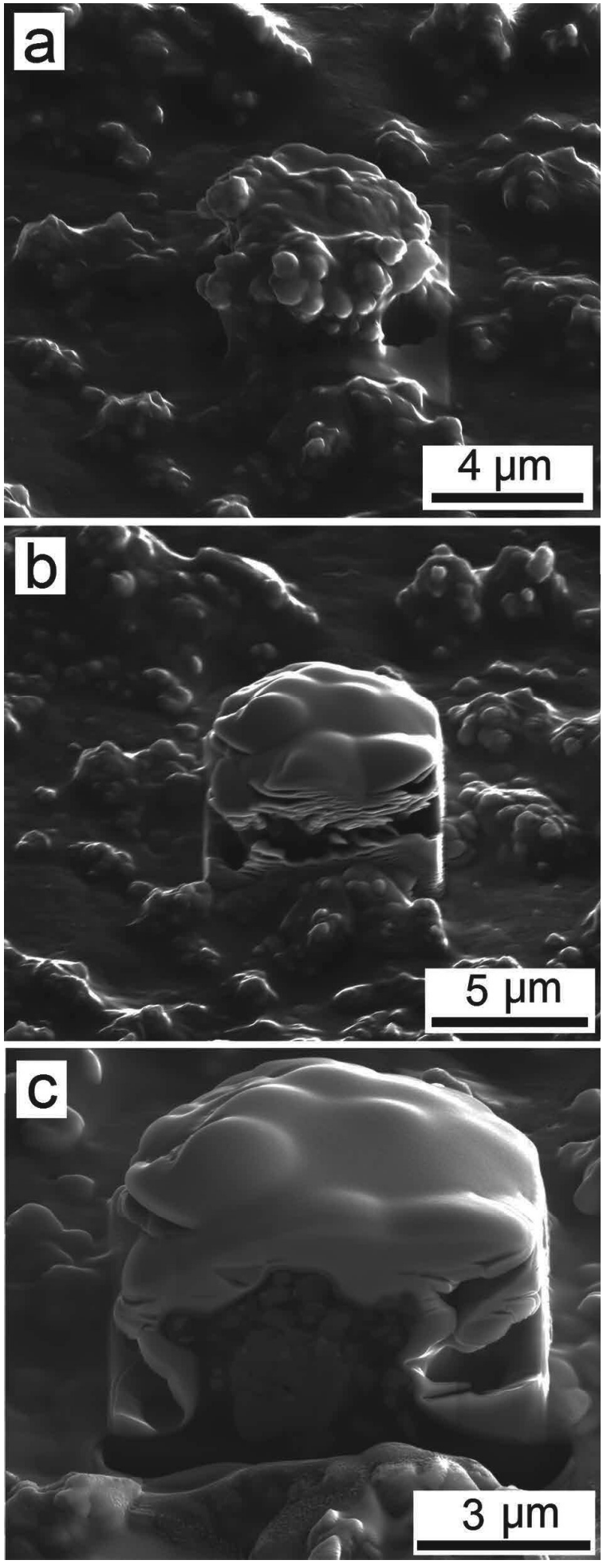
a
4 µm
b
5 µm
c
3 µm

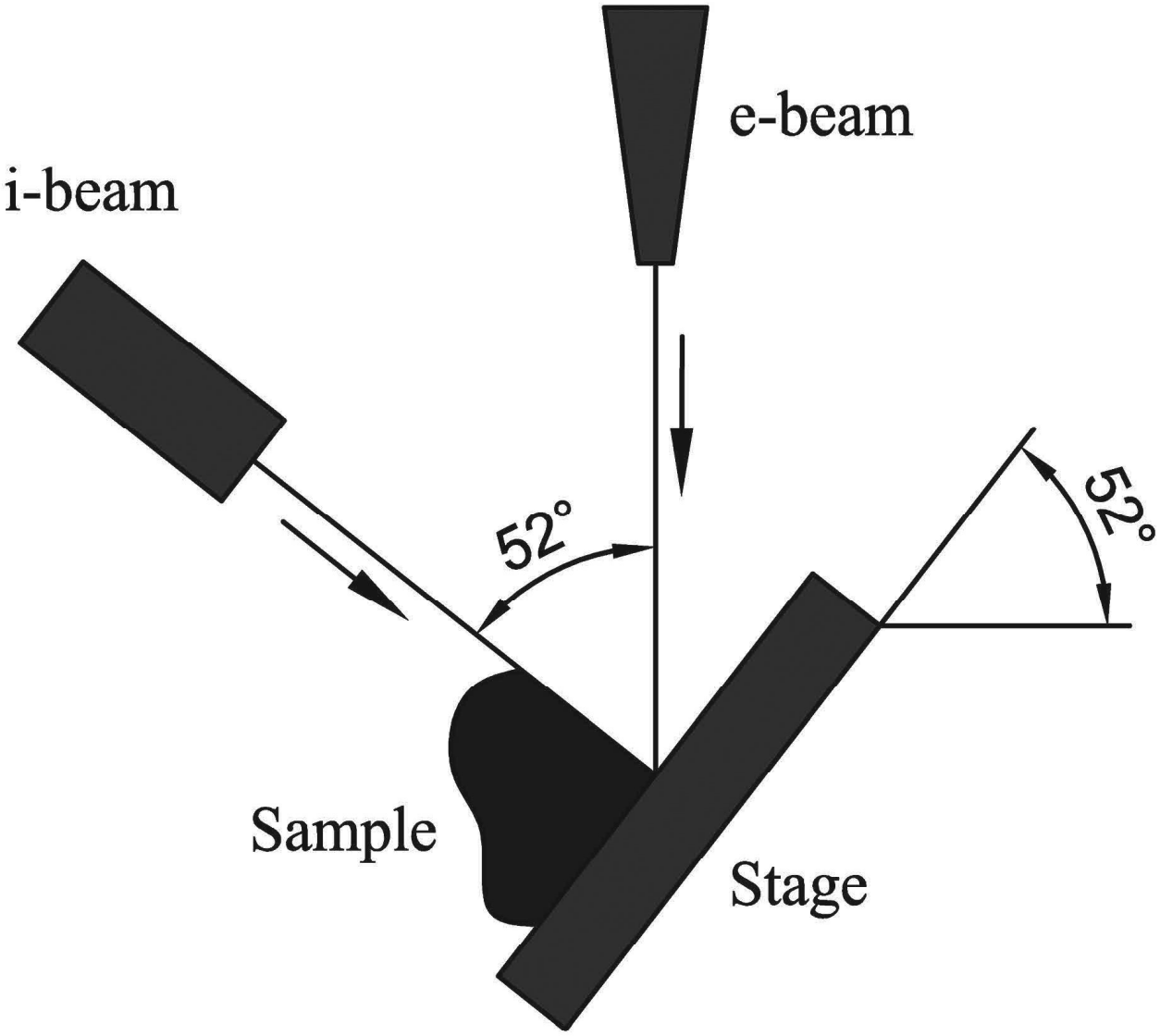
e-beam
i-beam
52°
52°
Sample
Stage

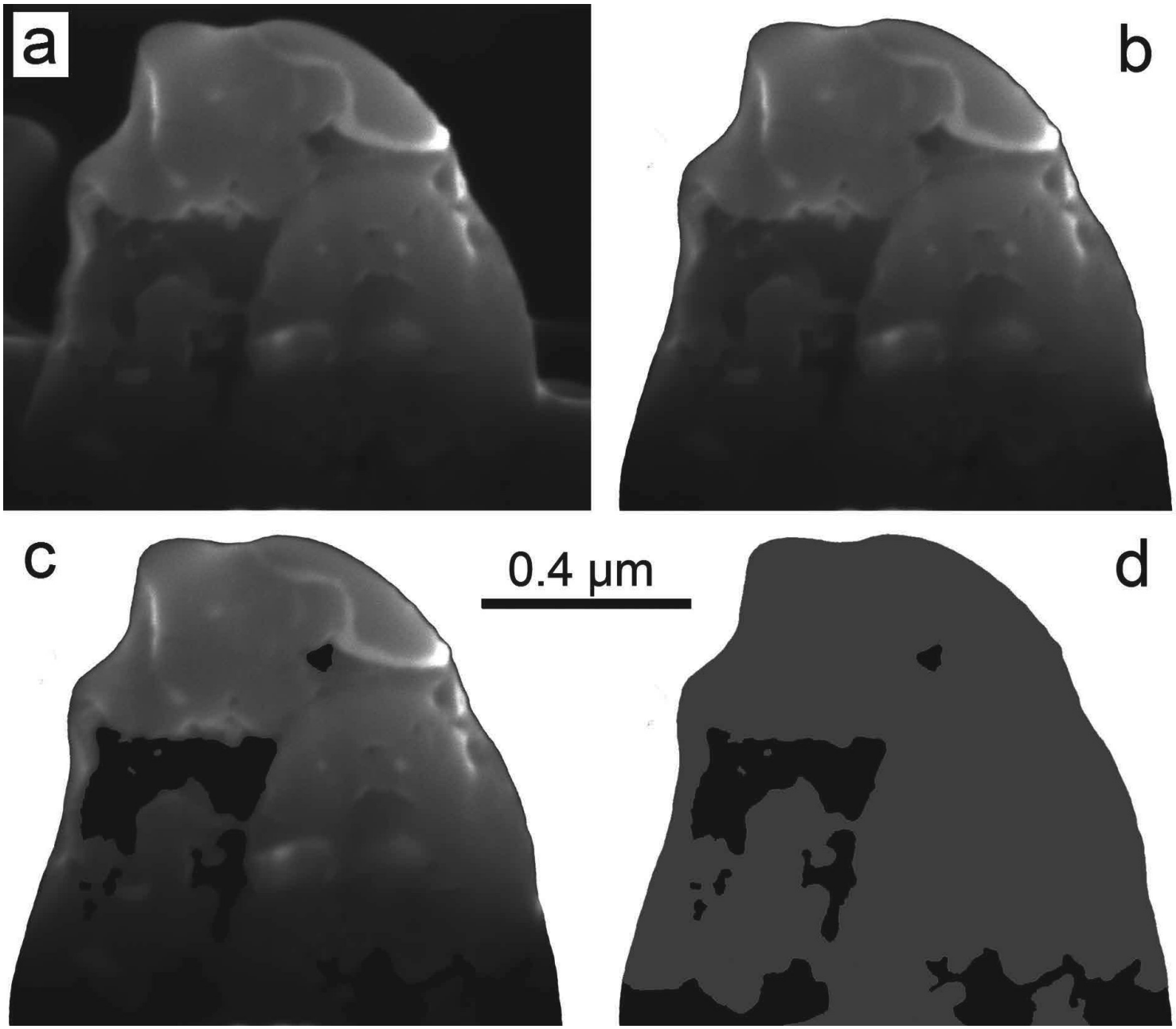
a
b
c
0.4 µm
d

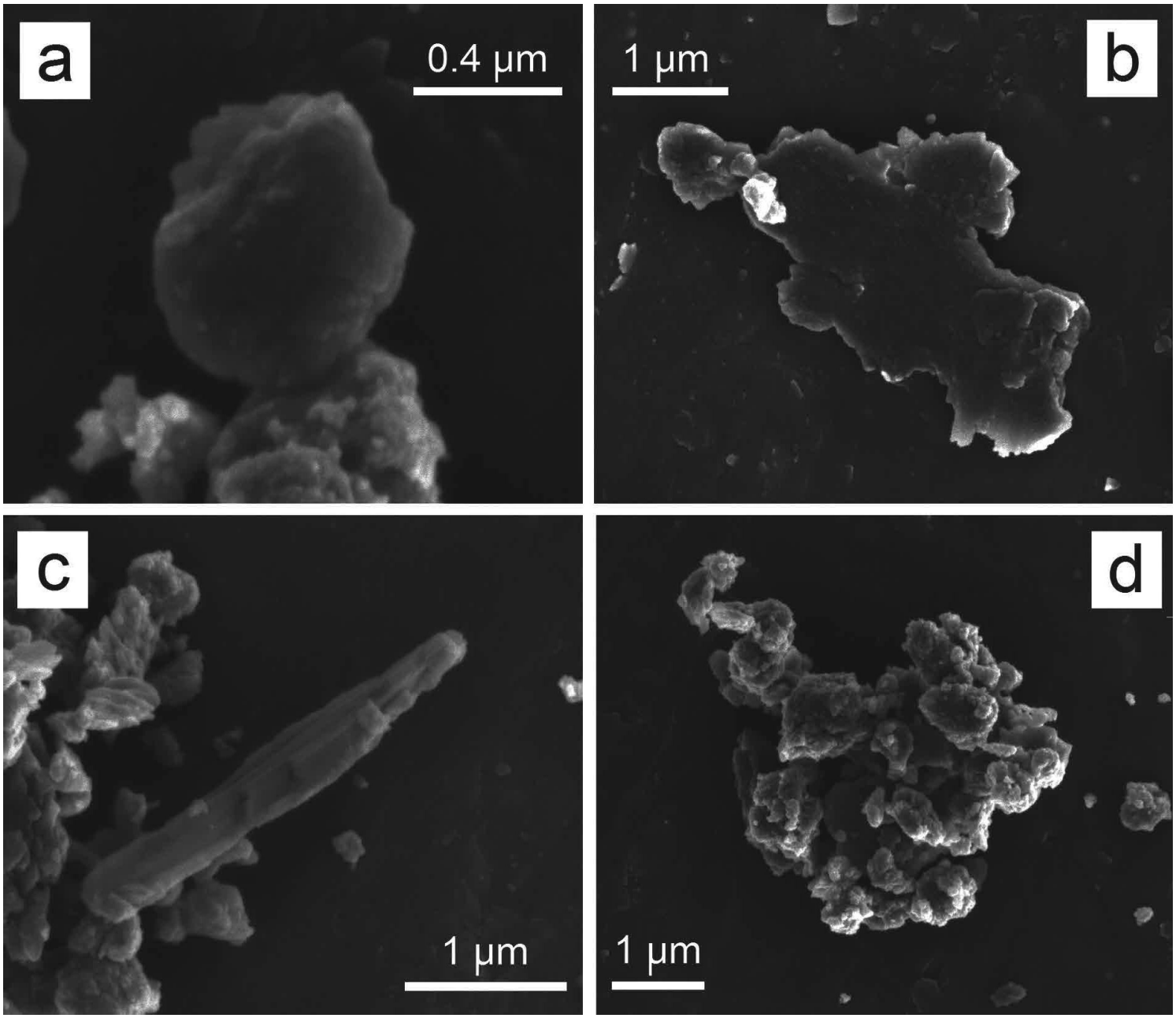
a
0.4 μm
b
1 μm
c
1 μm
d
1 μm

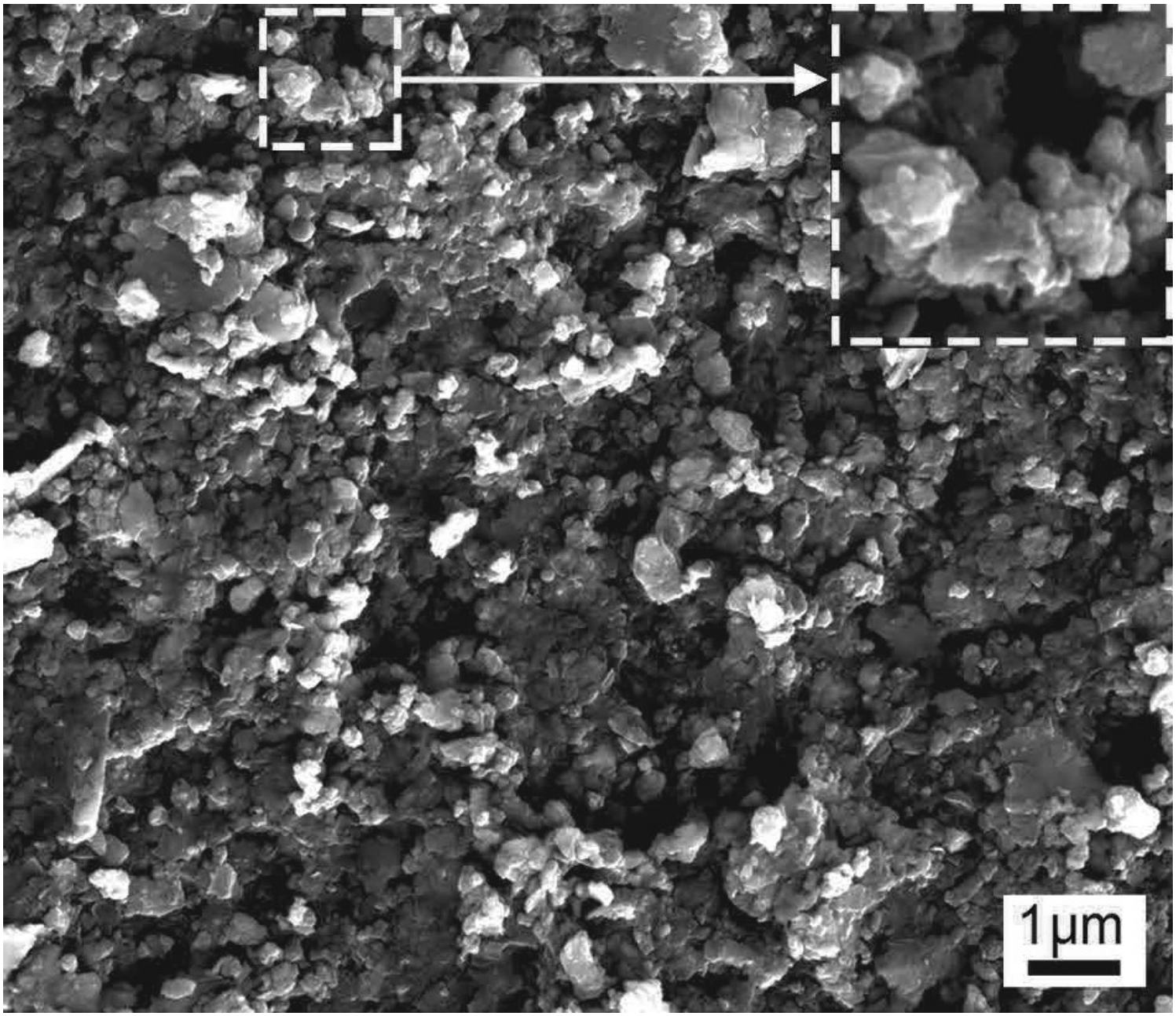
1μm

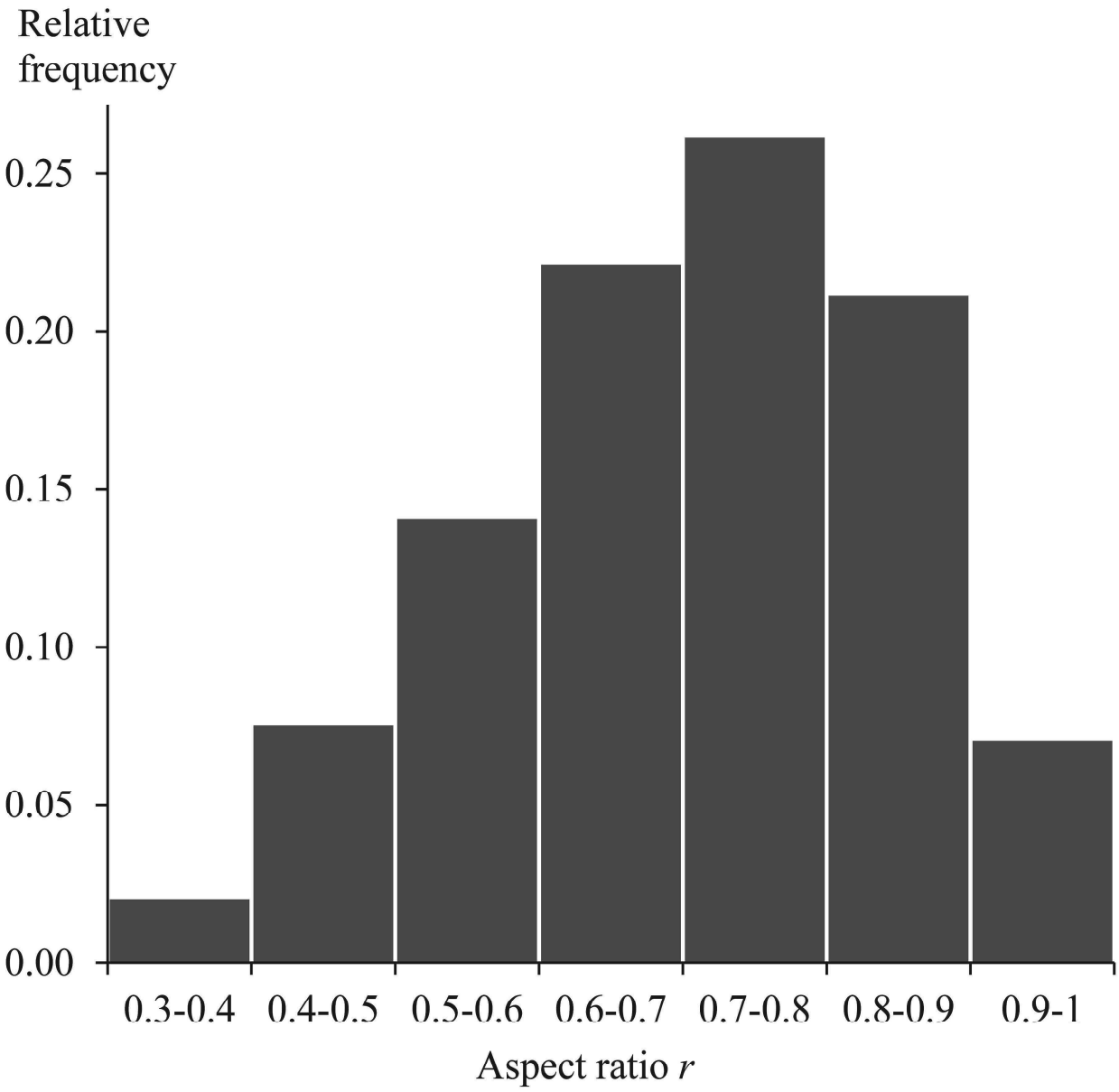
Relative
frequency
0.25
0.20
0.15
0.10
0.05
0.00
0.3-0.4
0.4-0.5
0.5-0.6
0.6-0.7
0.7-0.8
0.8-0.9
0.9-1
Aspect ratio r

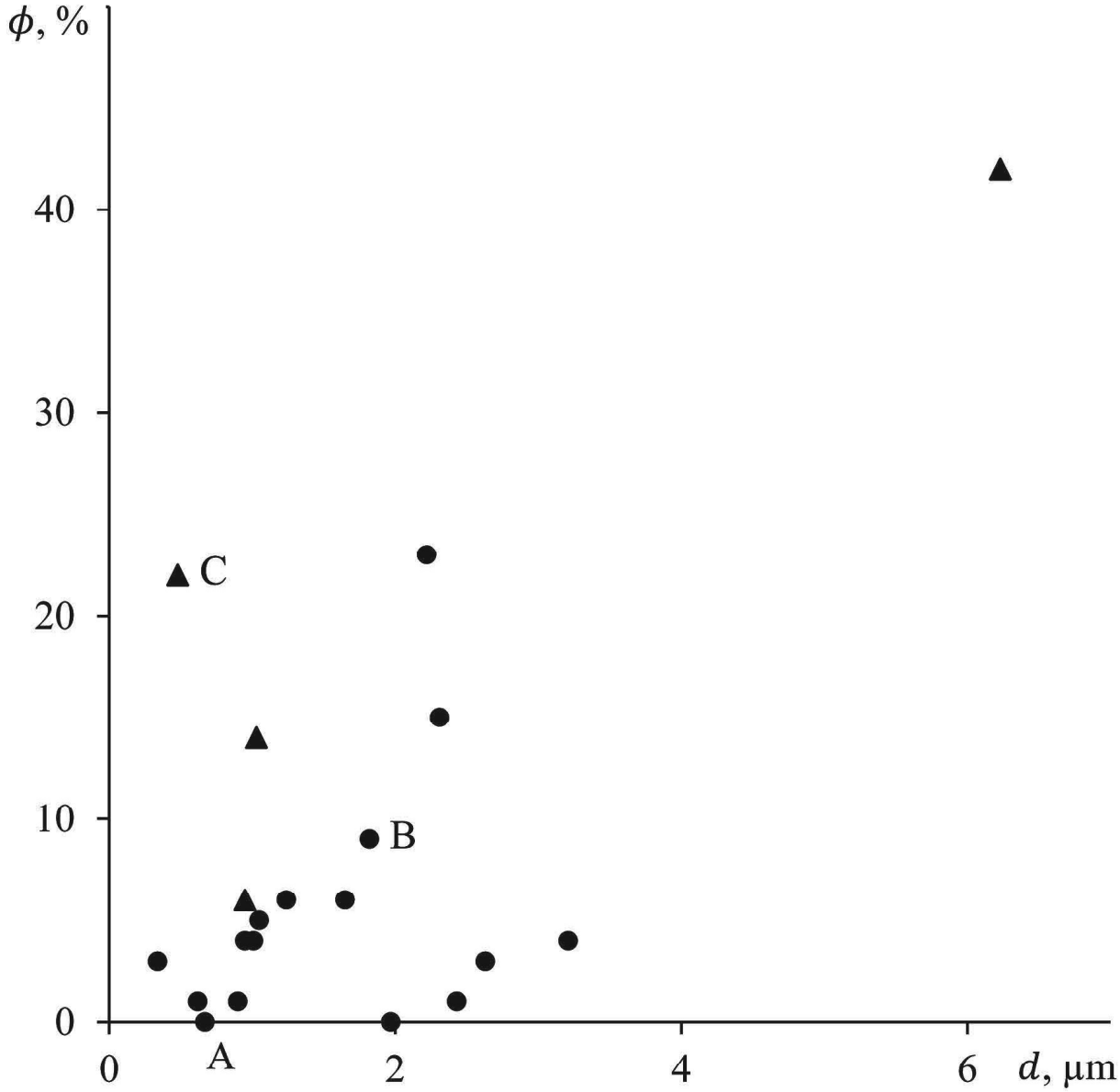
ϕ, %
40
30
20
10
0
C
B
A
0
2
4
6
d, μm

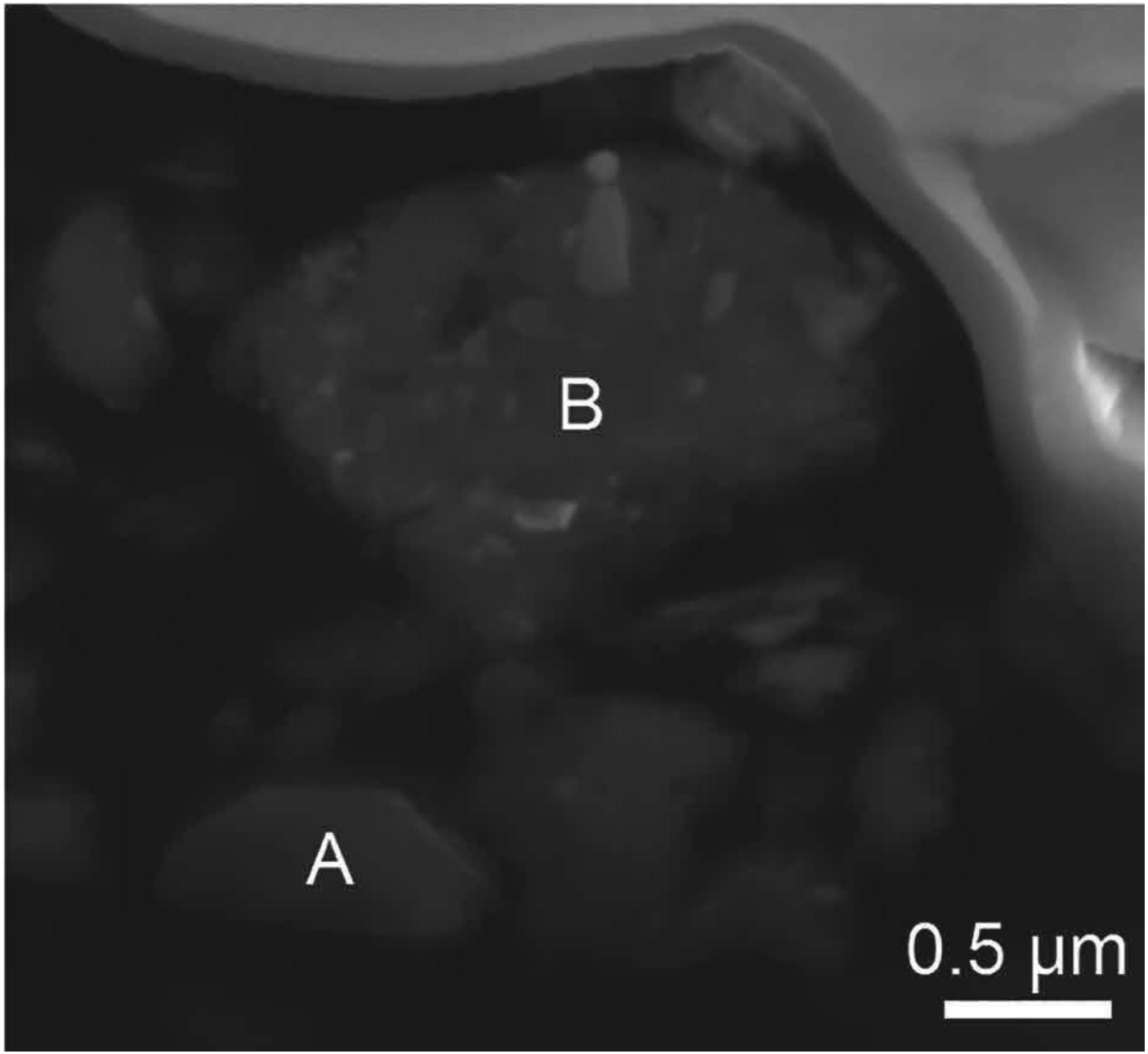
B
A
0.5 µm